Solid Freeform Fabrication 2016: Proceedings of the 27th Annual International Solid Freeform Fabrication Symposium – An Additive Manufacturing Conference
Reviewed Paper

Design and Realization of a 6 Degree of Freedom Robotic Extrusion Platform

Joseph R. Kubalak[1,2], Craig D. Mansfield[4], Taylor H. Pesek[3],
Zachary K. Snow[1], Edward B. Cottiss[1], Oliver D. Ebeling-Koning[3],
Matthew G. Price[1], Mark H. Traverso[1], L. David Tichnell[3],
Christopher B. Williams[1], Alfred L. Wicks[2]
[1]Design, Research, and Education for Additive Manufacturing Systems Laboratory
[2]Mechatronics and Autonomous Vehicles Laboratory
[3]Terrestrial Robotics Engineering and Controls Laboratory
Department of Mechanical Engineering
[4]Polymer Processing Laboratory
Department of Chemical Engineering
Virginia Tech
REVIEWED

Abstract

The layer-wise deposition of Additive Manufacturing (AM) processes allows for significant freedom in the design of product geometry; however, the use of 3-axis deposition tools results in layer interfaces that reduce material properties in the build direction. Adding additional degrees-of-freedom (DOF) to the AM tool could remove this limitation by enabling out of plane material deposition. For example, multi-DOF tool paths could align material extrusion with a part's stress contours to circumvent inter-layer delamination. As a step towards this goal, the authors designed, fabricated, and tested an AM extrusion system that leverages a 6-DOF robotic arm. In this paper, the authors detail the realization of this system including the design of a high-temperature filament extruder, kinematics and tool path generation, and user interface. The performance of the system is evaluated through layered deposition of ABS thermoplastic.

Key words: Material extrusion, Additive manufacturing, 3D printing, Industrial robot, Out of plane deposition

1. Introduction

Material extrusion is a classification of additive manufacturing (AM) that has found wide use by industry and hobbyists alike. In extrusion AM, a fluid (usually a softened thermoplastic) is precisely extruded onto a surface. The extrusion device and/or the build surface are moved such that the extruded material forms a single printed layer. As the motion control is typically accomplished via a 3-axis Cartesian coordinate platform, parts are formed by depositing successive layers along a vertical build axis.

While this method of layer-wise deposition has been shown to be capable of processing many different materials and realizing complex geometries, it does suffer from some limitations. The layer stacking discretizes curved surfaces, which due to the large layer thicknesses common with extruding viscous melts, results in a stair-stepping effect along the contour and

a poor part surface finish [1, 2]. Additionally, the extrudate cools rapidly upon deposition, leaving only a short window of time in which temperatures are elevated sufficiently for molecular diffusion across weld lines [3]. This poor weld strength results in anisotropic material properties along the build axis [2, 4]. To improve this weld strength, Partain investigated reheating the previous layer of the part just before depositing the current layer to encourage interlayer bonding [5]. Shaffer and coauthors added radiation sensitizers into filament and exposed the layer to radiation before depositing the next layer to promote crosslinking [6]. Perez developed specific polymer blends that showed less anisotropic behavior [7]. While these methods work for certain material types, they may not be universally effective.

Many groups have also looked to improve printed parts surface finish by creating adaptive slicing algorithms. By strategically adjusting the layer thickness used at different locations in the part (e.g., using smaller layers at places of higher curvature along the build axis), curves can be better approximated [8, 9]. Pandey et al. take a different approach by hybridizing the material extrusion process with machining technology to smooth stair-steps created in the deposition process [10]. Curved layer slicing was developed for 3-DOF systems so that the deposition path could better follow the curvature of the part [11–13].

Though means for improving the deposition strategies of material extrusion have been introduced, each of the above methods only work in very specific conditions. For instance, curved layer techniques have to be mindful of tool head and gantry collisions with the part being printed. Even with adaptive slicing, the surface is always discretized, and as the layer thickness continues to decrease, build time increases significantly.

To address prominent limitations found in extrusion AM, researchers are looking to move away from the 3-DOF gantry to more flexible printing platforms such as robotic arms or CNC tables with rotary platforms. Zhang et al. document the utility of robotic arms in a number of direct metal systems [14]. These high DOF systems have already been used to great effect in minimizing support material usage in Directed Energy Deposition AM processes [15–22]. Singh and Dutta have also shown that by changing the build direction throughout the part, the surface finish on a sloped or curving metal part can be improved [23]. Djuric and Urbanic have demonstrated the use of a robotic arm to deposit polymeric materials [24]. Though the work restricted the deposition strategy to XY layers, the authors do note the possibilities of more novel strategies. Keating and Oxman created a material extrusion platform using a robotic arm that carried a build platform between deposition and machining areas [25]. Mounting the platform to the robot allowed the printing of overhangs without the need for support by changing the orientation of the part relative to the deposition nozzle.

The authors here look to use the capabilities of a 6-DOF robotic arm to enable novel deposition strategies and process advanced composite polymers. As a step towards achieving this goal, this paper describes the design, fabrication, and testing of an extrusion AM platform that employs a 6-DOF robotic arm (ABB IRB 1200-7/0.7) [26]. Shown in Figure 1, the system features a custom built feed system and extruder, heated bed, and user interface. The system is built in Robot Operating Studio (ROS) [27] and accepts G-Code files from slicing software such as Slic3r [28]. The design of the system and its numerous sub-

functions, including filament feed system, extrusion hot end, control software, graphical user interface, path planning, and microcontrollers, are presented in Section 2. System validation is presented in Section 3, which includes demonstrations of part printing and measurements of part strength as a function of part orientation. A discussion of the resulting system is presented in Section 4. Closure and paths for future work are presented in Section 5.

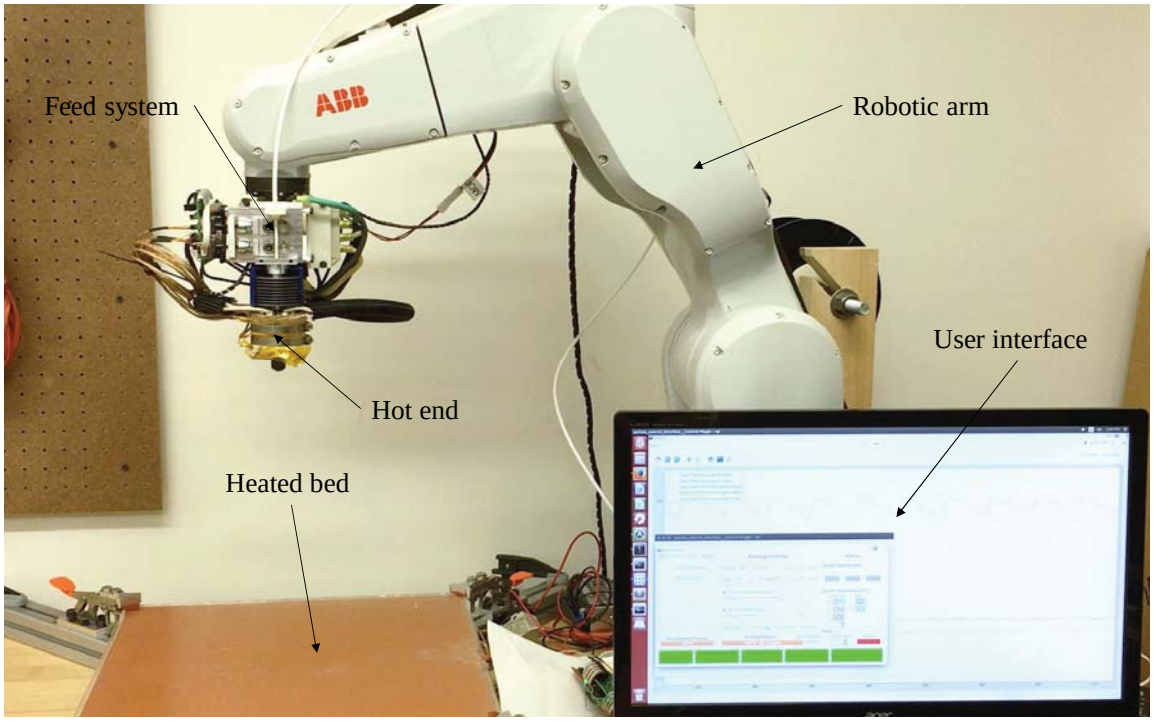

Figure 1: Robotic Material Extrusion Platform

2. System Design

This section outlines the design and fabrication of each subsystem of the material extrusion platform. The long-term goal for the platform is to develop novel deposition strategies by leveraging the capabilities of a 6-DOF robotic arm in conjunction with depositing polymer composite materials. No readily available slicing software has the capability to generate G-Code with Cartesian coordinates as well as tool orientation; as such new methods of slicing must be developed. Table 1 provides a concise list of the main requirements guiding the design of the robotic extrusion platform.

The following sections detail the design and implementation of the various subsystems comprising the platform.

2.1. Feed System

There are two different types of feed materials used in material extrusion processes, pellets and filaments. As previously mentioned, the platform is targeted toward printing composite materials which have continuous fiber reinforcement. This reinforcement restricts the design

Table 1: List of system design requirements

Design Requirements
Process 3mm filament
Able to reach melt chamber temperature of 350°C
Extrusion feed rate of 10 lb/hr
6-Axis (out of plane) Deposition
System accepts custom .gcode
Modular and expandable system architecture

to a filament fed system, as the screw mechanism required to process pellets would interfere with the continuous fiber.

Filament feed devices commonly feature a toothed gear driven by a motor, which forces feed material down the feed channel of the hot end and into a melt chamber. The completed feed system for the robotic material extrusion platform, shown in Figure 2, is based on that general concept. The one deviation is the inclusion of tandem knobbed gears, designed to maintain grip on filament through inconsistent diameter sections. This is particularly important for the processing of the small batch novel filaments, which are still in development and often result in inconsistent diameters. Opposing the knobbed gears are spring loaded bearings, which the user can tighten using the thumb screws on the side. The hot end mounts directly to the plate below the gears.

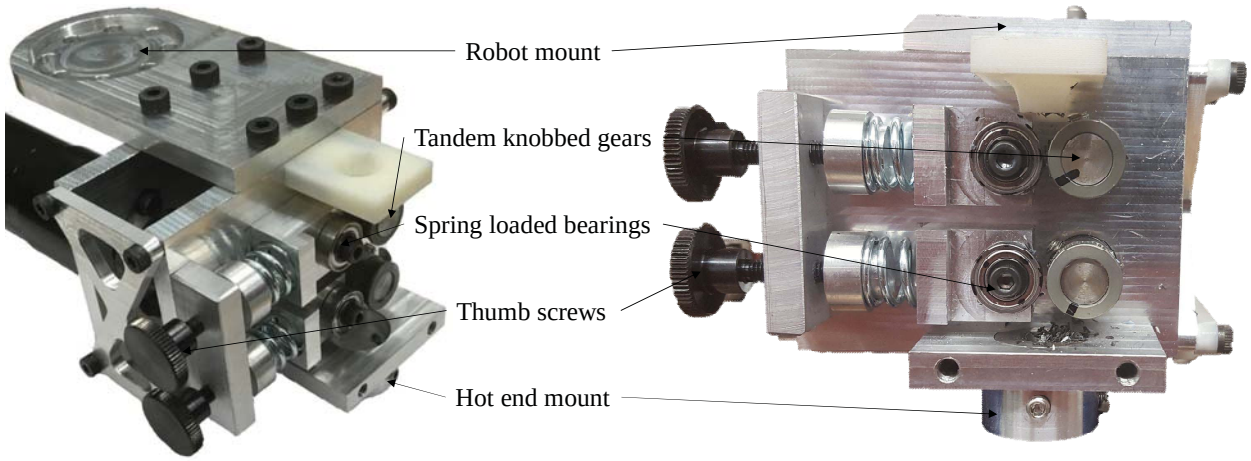

Figure 2: Isometric and front views of the assembled feed system

2.2. Hot End

The design for the hot end was based on the form found in most material extrusion applications: a heated section and a fin section separated by a heat break (Figure 3). The function of the heated section is to induce phase transition in the feed material. These elevated temperatures are required to reduce the viscosity of the melt, which improves both processability and print quality. However, if heat travels up the stock material outside of

the heated section, problems such as clogging the channel and buckling in the filament can occur. To prevent this, a fin section was designed with forced convective cooling.

Composite materials are typically more viscous than homogeneous materials and therefore require higher processing temperatures and pressure drops. To account for this, the feed channel was designed to take 3 mm feed stock. The 3 mm filament will have much more resistance to buckling in the feed system than 1.75 mm filament while also allowing for a wider range of nozzle diameters to work with during testing. For initial design validation and material property tests discussed in Section 3, a nozzle diameter of 2.25 mm was chosen for a 25% reduction.

The hot end was designed for printing 10 pounds of ABS an hour at 230°C with a maximum processing temperature of 350°C. In order to specify the appropriate heater size, a rough estimation of the power required to heat that output of ABS to the desired temperature was found to be 364 W. In order to achieve the maximum processing temperature, that estimate was approximately doubled. Six 100 W heaters are placed radially around the filament channel. Additionally, three thermocouples are placed up the length of the channel to monitor the temperature of the melt. The fully assembled hot end can be seen in Figure 3.

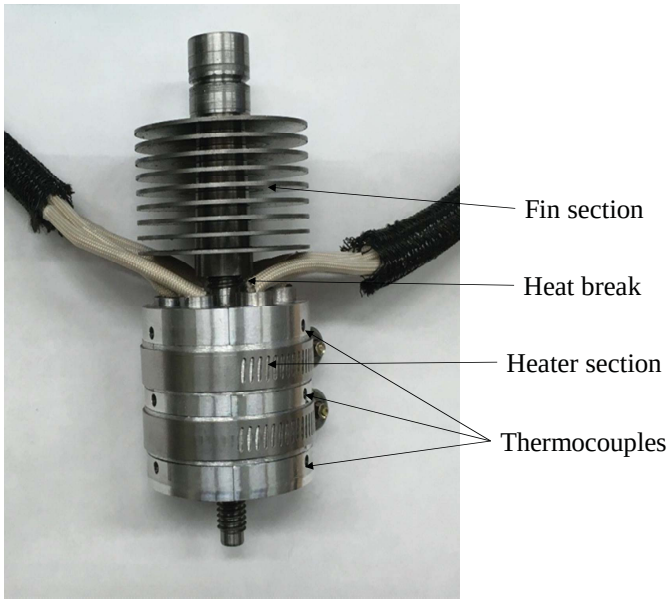

Figure 3: Fully assembled hot end

To validate the design as well as identify the necessary convective heat transfer coefficient across the fins, a thermal simulation was performed in Siemens NX 8.5. Properly specifying the coefficient is necessary to prevent melting from occurring inside the fin section, which can cause clogging and buckling. The simulation was performed with a 2D cross section with axial symmetry. Two of the 100 W heaters were modeled as modulated heat flux sources at their respective locations in the heating block. For this simulation, a convective heat transfer coefficient of 30 $\frac{W}{m^2 * K}$ was used across the fin section. A set point of 230°C (the

target temperature for processing ABS) was given to the bottom thermocouple with simple on-off control of the heaters. Figure 4 shows a resulting image from the simulation.

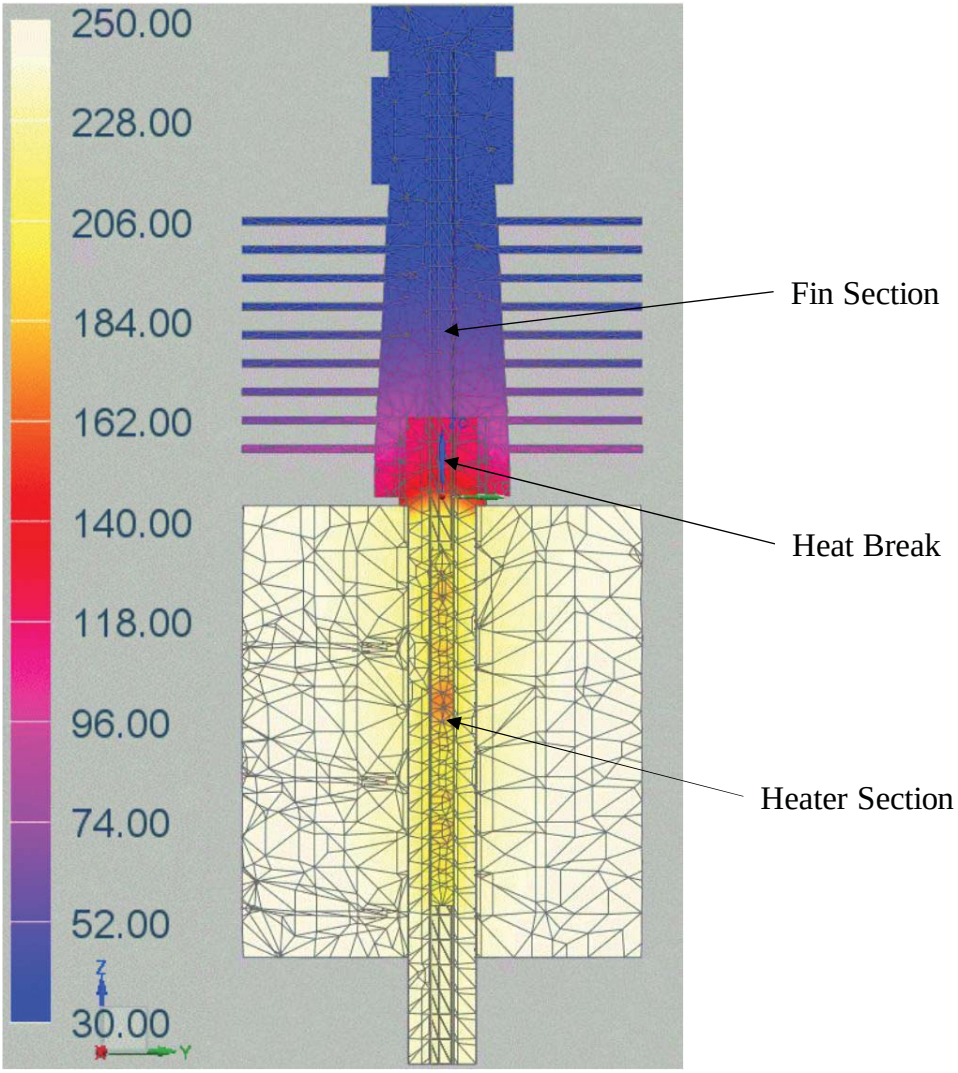

Figure 4: Hot end thermal simulation

As seen, temperature in the melt pool reaches approximately 220°C at the top and middle thermocouple and only reaches the desired 230°C at the location of the bottom thermocouple. To remedy this, a control scheme was developed to monitor both the top and bottom thermocouples. This setup provided adequate heating for printing while also not burning the extrudate.

The heat transfer coefficient of 30 $\frac{W}{m^2 * K}$ was found to provide sufficient cooling across the fins, appropriately dissipating the heat transferred through the heat break. The hottest temperature found above the heat break was approximately 100°C, just below the glass transition temperature of ABS.

2.3. Control Software

The system requires the integration of three subsystems: the main computer, robotic arm, and microcontrollers, which control the feed system motor and temperatures of the bed and hot end. The software architecture was built in ROS, which has a large open source community. Using ROS provides the ability to reuse large amounts of code from other sources, such as the ABB robot drivers and the MoveIt! motion planner.

Figure 5 shows a high-level software overview. For typical use, the user would first process the desired STL file through a slicing software to generate a G-Code file. This file then goes through a parser that pulls out movement and extrusion information. The information is converted into a tool path plan and sent to the robot. During a print, the robot is constantly tracking its own position and reporting it back to the main computer. Once the robot passes over the next point that was extracted from the G-Code, the computer sends the next extrusion command to the extruder.

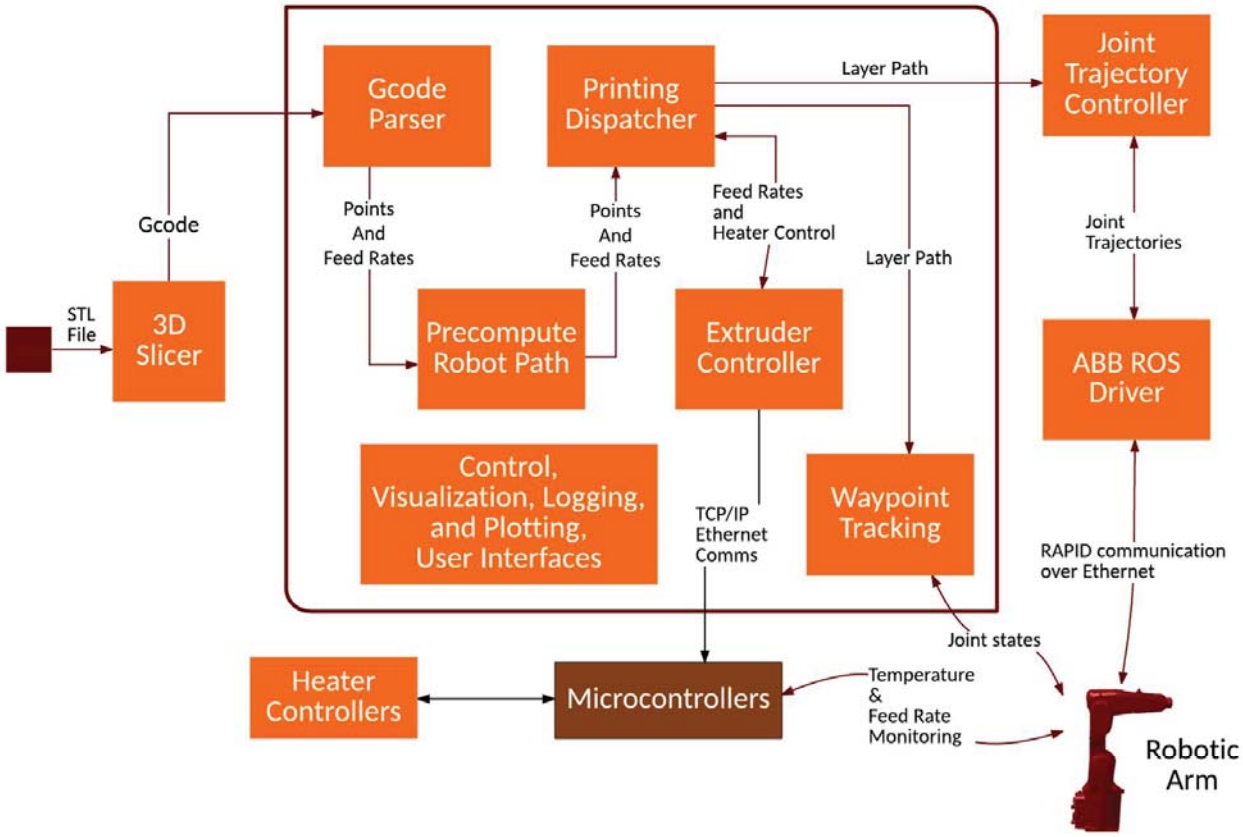

Figure 5: High level software flow chart

Building the system in ROS not only affords the ability to recycle previously used code but also inherently provides modularity to the system through its node based architecture [27]. Each functionality of the software is written as individual communicating nodes, which allows for integration of additional functionality, such as error detection, without a full overhaul of

the system. This isolation also allows for the use of different robotic arms, as the only robot specific nodes are the ABB drivers. Replacing this with a different brand or model of arm would transfer full system functionality to that new platform.

2.4. Graphical User Interface (GUI)

The GUI, shown in Figure 6, is where the user calibrates the robot, locates the file for printing, slices and generates the tool path, and begins the print. It also contains controls for the feed system and heaters. Additionally, there are a number of tools available to the user for monitoring the printer including thermocouple readouts for the extruder and bed and indicators signaling successful communication.

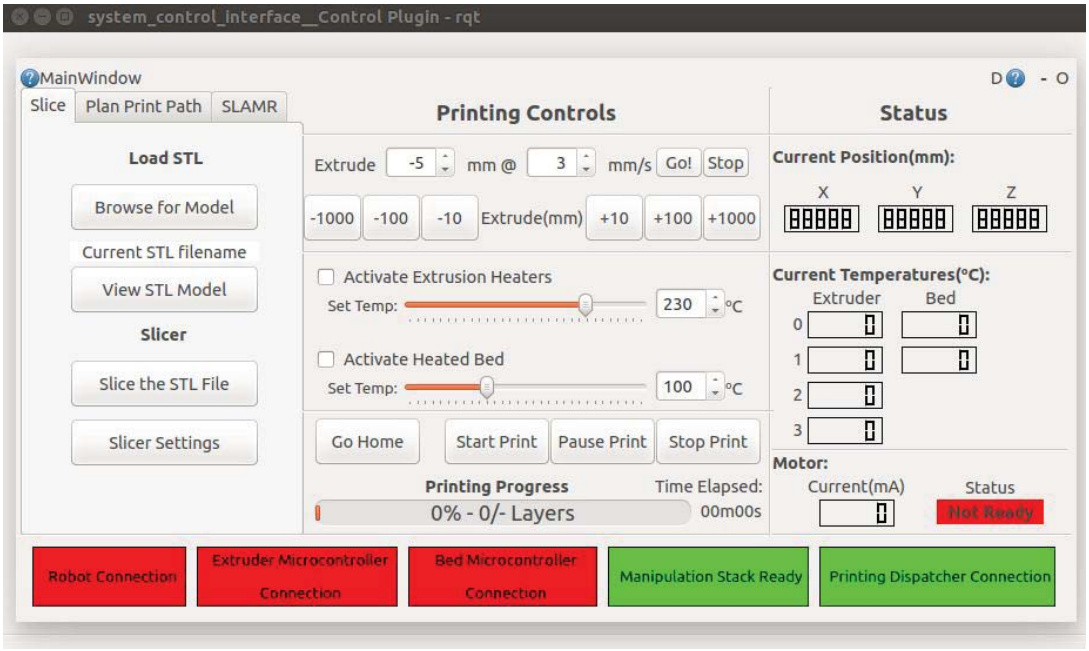

Figure 6: GUI used to control the platform

The most critical requirements for the control interface are stability and isolation. As it contains a number of safety features, the control interface cannot rely on other components of the system and it cannot crash during operation. The stop command available on the user interface is a safe stop for the system and will end the print. Though there are other methods of stopping the robot's movements and extrusion built into the system (including emergency stop buttons, a dead man switch, and power breakers), these methods have the potential to cause damage to the system if used improperly or during a print.

2.5. Path Planning

There are two options for generating a tool path for the robot: the XY planar deposition process demonstrated in Section 3 and the out of plane deposition process demonstrated in Section 6.

1. The XY planar deposition path planning operates exactly the same as most commercial printers. The user imports the desired STL file through the GUI and slices it, which produces a G-Code file. This can be done using a number of different slicers, but it is currently operating using Slic3r [28]. The user then selects to plan the tool path which performs all of the necessary inverse kinematics before printing can begin.

2. Out of plane deposition requires rotation information in addition to Cartesian coordinates. As such, a standard slicer is insufficient. To generate this tool path, the part is sliced flat on the bed as though it would be printed traditionally. The resulting G-Code and the desired part orientation is then passed to a custom MATLAB script that takes the orientation information, rotates the previously generated G-Code and creates a corresponding quaternion. The quaternion is then added to each move command in the G-Code. This new G-Code file can then be imported to the GUI where the user can initiate the same path planning algorithms used in the XY path planning approach.

2.6. Microcontroller

The designed system uses two microcontrollers to communicate between the end effector, the heated bed, and the main computer. The system required communication over TCP/IP, SPI, CAN, and I/O switching capabilities, as such, the TI TIVA TM4C1294XL microcontroller was selected. Interfacing with the microcontrollers were a number of peripherals: K-type thermocouples, EPOS 2 motor controller, and heater relay control. The thermocouples are used to measure the hot end melt chamber temperatures in three locations and the heated bed in two locations. The EPOS 2 motor controller drives the Maxon motor used in the feed system. The relays control the power to the heated bed and hot end. As there were no existing boards to interface with the microcontroller and desired peripherals, a custom shield, shown in Figure 7, was designed as a compact solution.

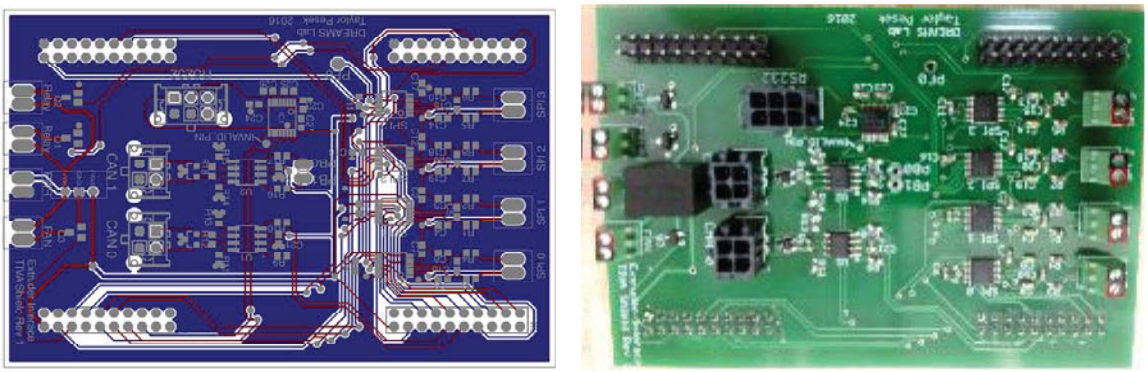

Figure 7: Custom shield for the TIVA microcontroller as designed (left) and produced (right)

Basic temperature control is achieved by switching the relay on and off around maximum and minimum temperature set points. As an additional safety feature on the extruder side,

another relay is used as an enable relay in conjunction with the main heat control relay. This is in response to relays being mechanical devices with a limited number of switching cycles. If the control relay broke closed during a print, the uncontrolled temperature rise could potentially damage the hot end. The enabling relay switches on when first turning on the heaters and will switch off if any anomalies are detected in the switching of the control relay.

3. System Validation

3.1. Base Functionality

Initial tests were performed in stages. After communication between the computer, microcontrollers, and robot was established, basic extrusion tests without robot movement were performed. This was to ensure proper heating of the filament and sufficient cooling across the fins. Figure 8 shows temperature data from the top hot end thermocouple during the simple extrusion test with a set point of 240°C.

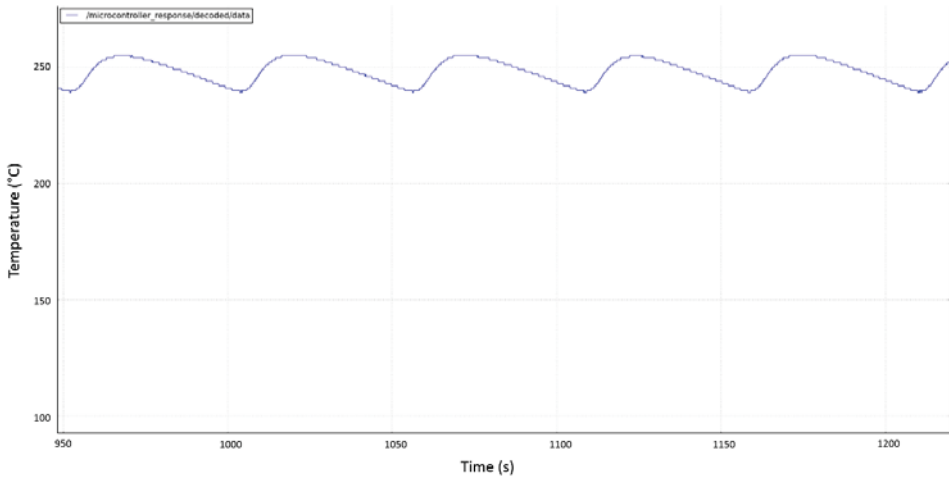

Figure 8: Steady state temperature data of the top hot end thermocouple while printing

The temperature creates a periodic pattern around 250°C where the heaters are switched on when drifting slightly below the set point, overshooting, and then finally cooling down. This is due to the distance between the heaters and thermocouples, which causes the heaters to heat the area around them faster than the temperature rise registers at the thermocouples. A more advanced control scheme that accounts for the delay has been developed but not tested. Next, basic print parameters, shown in Table 2, were found empirically. This configuration was used to create the sample prints shown in Figure 9.

Table 2: A list of the most relevant print parameters used for making the tensile specimens

Parameter Name	
Layer Height	1.4 mm
Perimeter Speed	10 mm/s
Infill Speed	20 mm/s
Non-print Speed	40 mm/s
Bed Temperature	100°C
Extruder Temperature	235°C
Skirt Loops	2 (1 for Z)

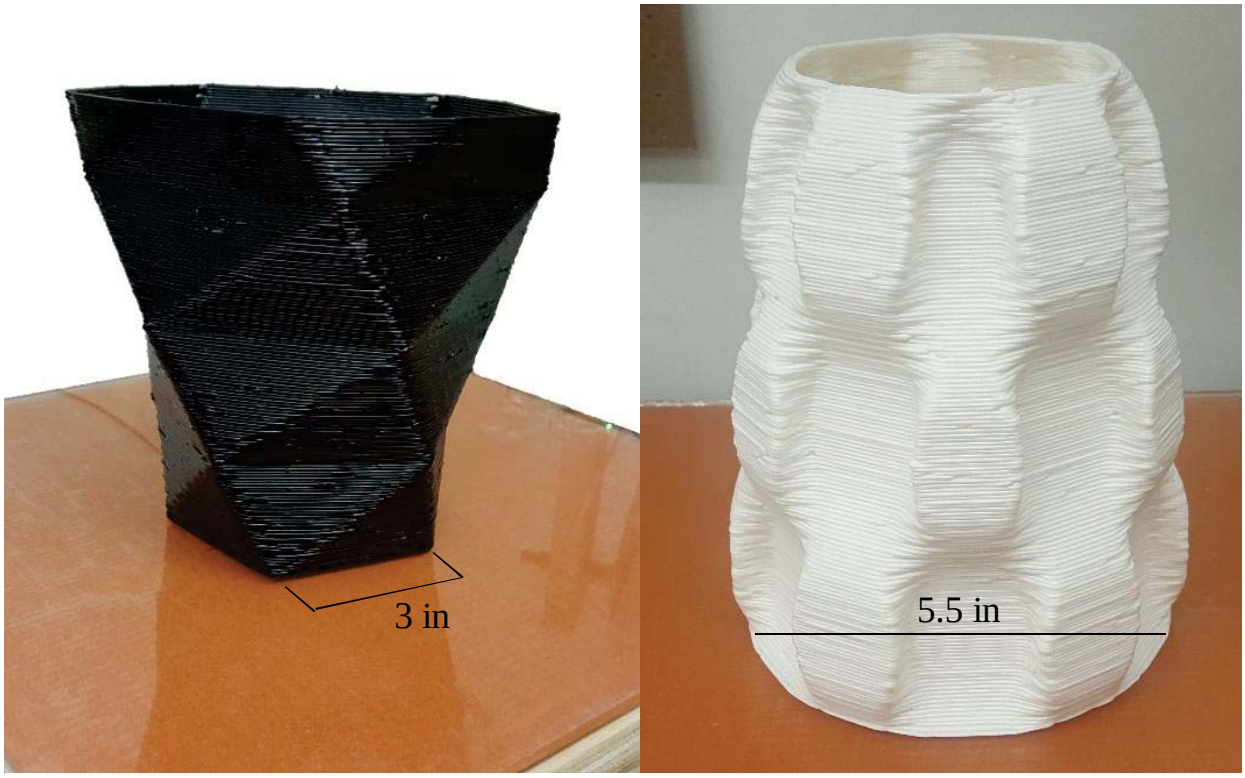

Figure 9: Sample prints from the robotic extrusion platform

3.2. Mechanical Property Testing

3.2.1. Testing Methods

System performance was verified through tensile strength tests on directly printed specimens in accordance with ASTM D638 [29]. Three tensile specimens, each with an overall length of 165 mm, were printed with the robotic material extrusion system in each Cartesian direction using ABS plastic. All specimens were printed with infill roads strictly in the X direction. The first layer of each specimen type is shown in Figure 10. An extruded "skirt" was used to clear out the nozzle to ensure the quality of extrudate during printing. The specimens were created using the previously established print parameters. System calibration and material spool were also kept constant throughout the test.

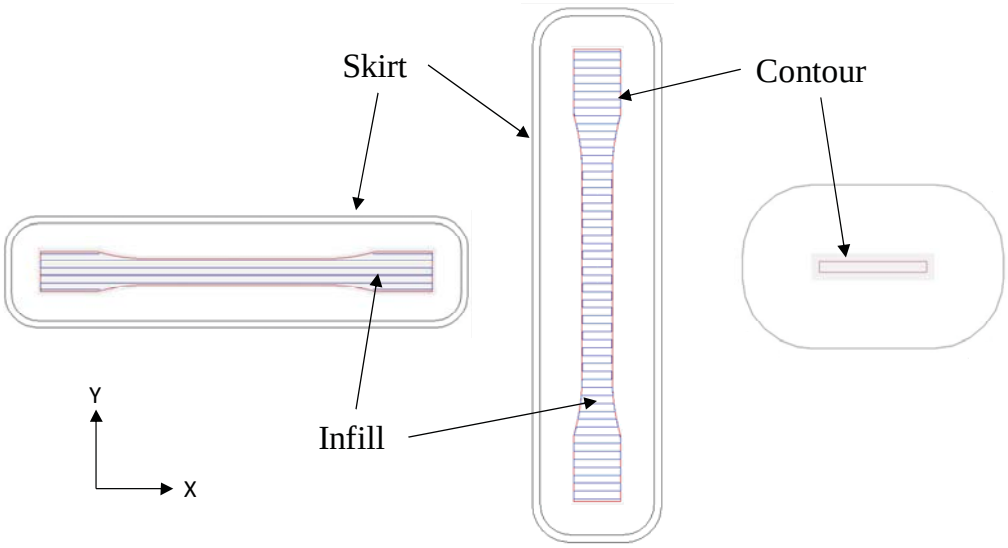

Figure 10: The first layer of each specimen type: X (left) Y (center) Z (right)

Due to the small cross sectional area of the Z specimens, the recently finished layer and those below it were still soft when beginning the next layer. As these layers continued to stack up, the specimen lost all shape and stability, causing the build to quickly collapse. To prevent this, a delay of 20 seconds was placed after each layer to allow the specimen to sufficiently cool for the subsequent layer. This delay allowed the nozzle to ooze filament, compromising the beginning of the next layer. In response, the same skirt used in the first layer was placed at the beginning of each layer to allow the nozzle to clear itself. This had the added benefit of creating additional support structure, shown in Figure 11, for the specimen as it grew. The thickness of the specimen was also reduced in order to eliminate the need for infill, as the infill roads were also found to compromise the quality of the specimen.

The Z specimen did require post processing in the form of removal from the stacked skirts. The threads connecting it to the skirts were cut and excess material threads were removed. The X and Y specimens were able to be tested as printed with no additional processing. Figure 12 shows a printed specimen of each type.

Figure 11: Z specimen as printed. The stacked skirts allow the nozzle to clear while also supporting the specimen

Figure 12: Specimens as printed, each with an overall length of 165 mm.
X (top) Y (middle) Z (bottom)

3.2.2. Testing Results

The tensile tests were performed on an Instron 5894 and followed ASTM D638 [29]. The Z specimens broke too quickly for proper measurement with the standard 5 mm/min extension rate, so a rate of 2 mm/min was used for those tests. An extensometer was attached to the gauge section of each specimen during testing. Stress-strain curves for all specimens are shown in Figure 13.

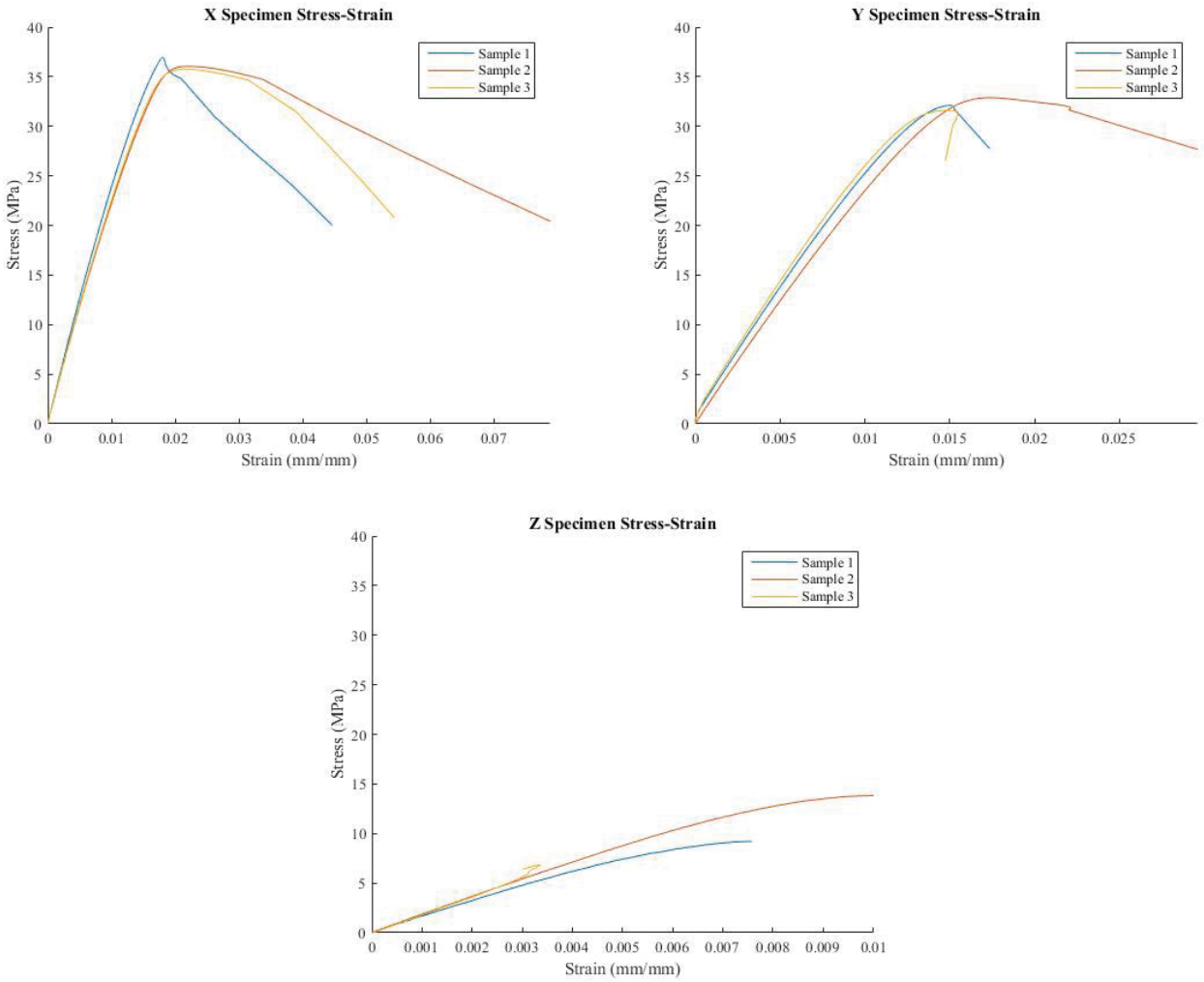

Figure 13: Stress-strain curves for all tensile specimens

The modulus was calculated using a linear fit through the data set. The amount of data used in the linear fit was reduced until the R squared value exceeded 0.995. Yield strengths were calculated using the Offset Yield Strength method described in ASTM D638 with an offset of 0.2%, the results of which are shown in Figure 14 [29]. The "aligned" data set presents data from samples similar to the X specimen set with roads aligned down the length of the tensile specimen [30].

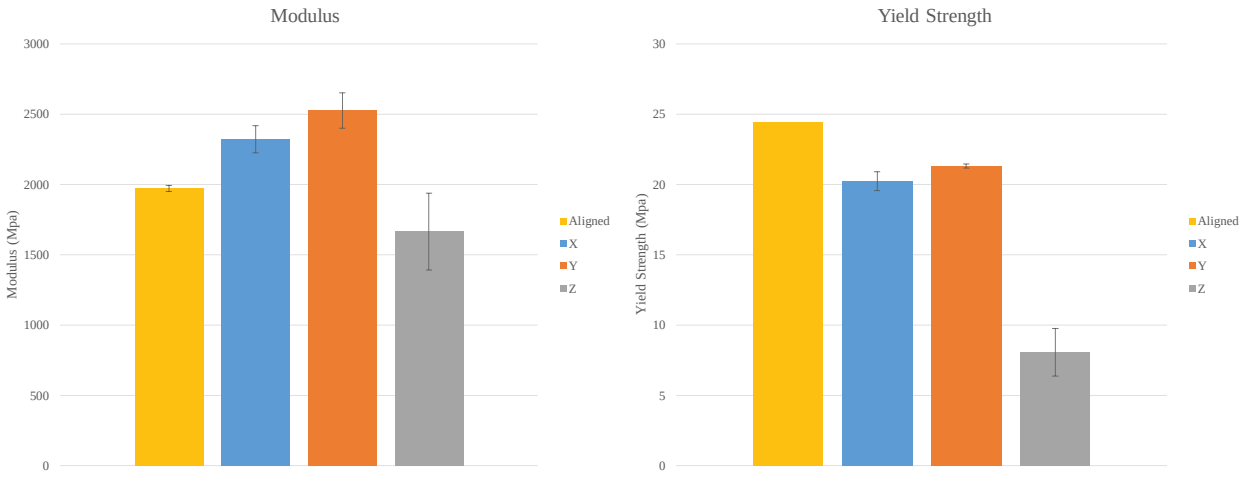

Figure 14: Moduli and yield strength results

4. Discussion

The results of the tensile tests were as expected. The in-plane strength is much greater than that of the out of plane strength. The one discrepancy from expectation is the better performance of the Y specimens over the X. This is a result of the following:

1. The layers in the Y specimens were deposited more quickly than the X specimens. The tool path for the X specimens was such that a number of travel (non-printing) moves were required to complete a layer. These travel moves add additional time per layer, allowing the part to cool, which limits interlayer diffusion during deposition. This is in contrast with the tool path for the Y specimen, which only had two travel moves per layer: a move from the end of the contour to the start of the infill and a move from the end of the infill to the start of the next contour.

2. The infill pattern of the Y specimens reinforced the contour. During deposition of the contour for each layer, a small gap was occasionally created where the start and end points of the extrusion did not overlap, creating a weak point. This event occurred in all specimens, but the Y specimens were able to compensate for the gaps with infill.

3. The infill pattern consisted of many short roads. This allowed for enhanced bonding between the roads in the Y specimens over the X specimens, as those roads were much longer and therefore had additional time to cool before an adjacent road was placed. A part will not necessarily have exclusively short roads, so the performance of the Y specimens may be inflated.

These concerns all pertain to the way in which the specimens were produced. By keeping the fabrication method (i.e. the tool path) the same between the X and Y specimen sets, these issues would not appear. As such, future testing should examine these same properties from samples machined from a printed sheet.

An additional point of note is the inconsistency in the Z specimens. Figure 14 shows that the yield strength standard deviation is 2.5 times greater in the Z direction than in the X direction. This variation results from two causes:

1. The printer resolution. The XY cross sectional area of the Z specimens (3.49 mm by 19 mm in the grip section) is close to the nozzle diameter (2.25 mm) of the printer, thus requiring only two passes per layer. The tool path nominally takes the form of a rectangle, but as the robot makes the sharp corners at each end the cross section is rounded into an oval.

2. The fabrication method. The road cross-sectional area is much larger on this platform than those from a traditional material extrusion system. As such, they retain heat longer. Though this behavior is beneficial for inter-road bonding, it also compromises print quality for small prints such as this. The artificial delays between layers were necessary to have a survivable sample, but greatly reduce the potential for layer bonding. That said, the delays were also not long enough for the previous layer to fully cool, causing it to deform during the deposition of the next layer. This further exacerbates the resolution issue by warping the cross section.

Both of these issues are prevented with a larger layer. The print time per layer increases and the resolution issues caused by the large nozzle are diminished with larger travel times. As such, machining the Z specimens from a block of material rather than directly printing them may give a better estimate of the material properties one could expect from a print.

5. Conclusion and Future Work

This paper detailed the design, fabrication, and testing of a robotic material extrusion platform. The custom extruder and feed system are shown to be capable of processing ABS plastic. The system is capable of processing standard G-Code files output from slicing software and realizing complex structures such as those seen in Figure 9. Material tests have also shown that the printed ABS is, expectedly, anisotropic with an in-plane yield strength of 20 MPa, 50% of the nominal strength.

The presented platform is designed to extend the capabilities of typical 3-DOF AM extrusion by leveraging a 6-DOF robotic arm. The additional DOF provide the ability to rotate the tool head, allowing for out of plane deposition. An example of this can be seen in Figure 15. Sacrificial scaffolding structures were deposited in the XY plane, but the model material was deposited at an angle, normal to the surface of the desired part.

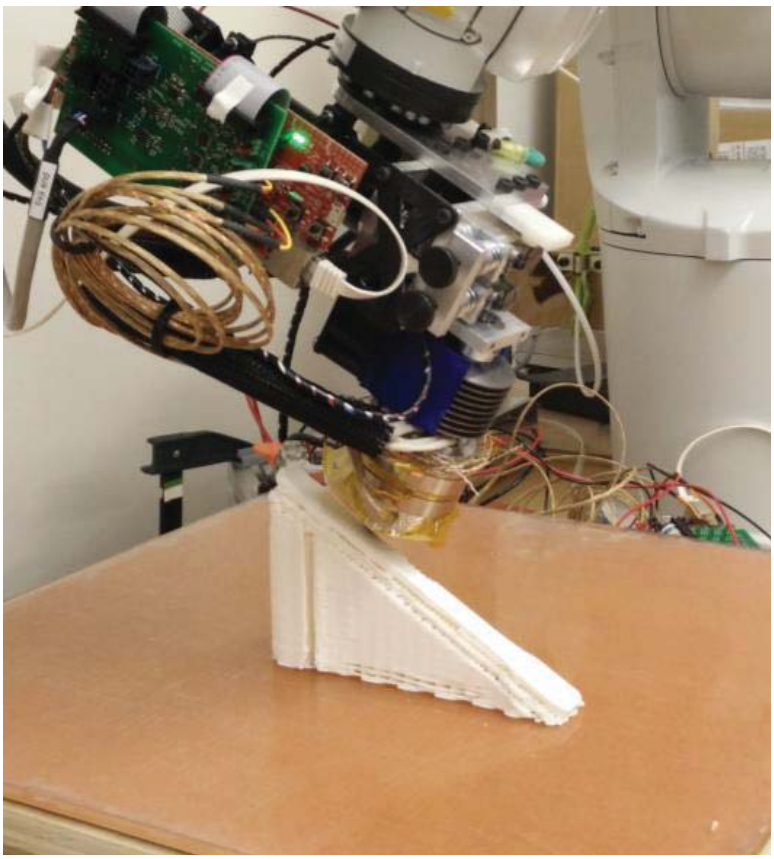

Figure 15: Tensile specimen printed using out of plane deposition techniques

This idea can, as previously established, eliminate the stair-stepping effect in a number of parts, but also improve material properties. As seen, the tool path of the desired object resembles that of the X specimens discussed in this paper. This is opposed to if the object was printed with a 3-DOF gantry, where the tool path would much more closely resemble that of the Z specimens. As discussed, the X specimens dramatically outperformed the Z specimens. The authors feel there is potential for similar behavior with out of plane deposition.

References

[1] M. K. Agarwala, V. R. Jamalabad, N. A. Langrana, A. Safari, P. J. Whalen, and S. C. Danforth, "Structural quality of parts processed by fused deposition," *Rapid Prototyping Journal*, vol. 2, no. 4, pp. 4–19, 1996.

[2] B. N. Turner, R. Strong, and S. a. Gold, "A review of melt extrusion additive manufacturing processes: I. Process design and modeling," *Rapid Prototyping Journal*, vol. 20, no. 3, pp. 192–204, 2014.

[3] J. E. Seppala and K. D. Migler, "Infrared thermography of welding zones produced by polymer extrusion additive manufacturing," *Additive Manufacturing*, 2016.

[4] S.-H. Ahn, M. Montero, D. Odell, S. Roundy, and P. K. Wright, "Anisotropic material properties of fused deposition modeling ABS," *Rapid Prototyping Journal*, vol. 8, no. 4, pp. 248–257, 2002.

[5] S. C. Partain, "Fused deposition modeling with localized pre-deposition heating using forced air," Master's thesis, Montana State University, 2007.

[6] S. Shaffer, K. Yang, J. Vargas, M. A. Di Prima, and W. Voit, "On reducing anisotropy in 3D printed polymers via ionizing radiation," *Polymer*, vol. 55, no. 23, pp. 5969–5979, 2014.

[7] A. R. Torrado Perez, *Defeating Anisotropy in Material Extrusion 3D Printing Via Materials Development*. PhD thesis, University of Texas at El Paso, 2015.

[8] J. Tyberg and J. H. Bohn, "Local Adaptive Slicing," *Rapid Prototyping Journal*, vol. 4, no. 3, pp. 118–127, 1998.

[9] R. L. Hope, R. N. Roth, and P. A. Jacobs, "Adaptive Slicing with Sloping Layer Surfaces," *Rapid Prototyping Journal*, vol. 3, no. 3, pp. 89–98, 1997.

[10] P. M. Pandey, N. V. Reddy, and S. G. Dhande, "Improvement of surface finish by staircase machining in fused deposition modeling," *Journal of Materials Processing Technology*, vol. 132, 2003.

[11] D. Chakraborty, B. A. Reddy, and A. R. Choudhury, "Extruder path generation for Curved Layer Fused Deposition Modeling," *Computer-Aided Design*, vol. 40, pp. 235–243, 2008.

[12] R. J. Allen and R. S. Trask, "An experimental demonstration of effective Curved Layer Fused Filament Fabrication utilising a parallel deposition robot," *Additive Manufacturing*, vol. 8, pp. 78–87, 2015.

[13] B. Huang and S. Singamneni, "Curved Layer Adaptive Slicing (CLAS) for Fused Deposition Modeling," *Rapid Prototyping Journal*, vol. 21, pp. 354–367, 2015.

[14] G. Q. Zhang, X. Li, R. Boca, J. Newkirk, B. Zhang, T. A. Fuhlbrigge, H. K. Feng, and N. J. Hunt, "Use of industrial robots in additive manufacturing - A survey and feasibility study," in *Proceedings of 41st International Symposium on Robotics*, pp. 512–517, 2014.

[15] J. Ruan, K. Eiamsa-ard, and F. Liou, "Automatic Process Planning and Toolpath Generation of a Multiaxis Hybrid Manufacturing System," *Journal of Manufacturing Processes*, vol. 7, no. 1, pp. 57–68, 2005.

[16] J. Ruan, T. E. Sparks, A. Panackal, F. W. Liou, K. Eiamsa-Ard, K. Slattery, H. N. Chou, and M. Kinsella, "Automated slicing for a multiaxis metal deposition system," *Journal of Manufacturing Science and Engineering, Transactions of the ASME*, vol. 129, no. 2, pp. 303–310, 2007.

[17] K. Lee and H. Jee, "Slicing algorithms for multi-axis 3-D metal printing of overhangs," *Journal of Mechanical Science and Technology*, vol. 29, no. 12, pp. 5139–5144, 2015.

[18] W. Xiangping, Z. Haiou, W. Guilan, and W. Lingpeng, "Adaptive Slicing for Multi-axis Hybrid Plasma Deposition and Milling," *Solid Freeform Fabrication Symposium*, pp. 1277–1287, 2015.

[19] D. Ding, Z. Pan, C. H, N. Li, and S. v. D. Larkin, "Multi-Direction Slicing of STL Models for Robotic Wire-Feed Additive Manufacturing," *Solid Freeform Fabrication Symposium*, vol. XXXIII, no. 2, pp. 1059–1069, 2015.

[20] J. Zhang and F. Liou, "Adaptive Slicing for a Multi-Axis Laser Aided Manufacturing," *Journal of Mechanical Design*, vol. 126, 2004.

[21] R. Dwivedi and R. Kovacevic, "Process Planning for Multi-Directional Laser-Based Direct Metal Deposition," *Proceedings of the Institution of Mechanical Engineers, Part C: Journal of Mechanical Engineering Science*, vol. 219, no. 7, pp. 695–707, 2005.

[22] W. C. Lee, C. C. Wei, and S. C. Chung, "Development of a hybrid rapid prototyping system using low-cost fused deposition modeling and five-axis machining," *Journal of Materials Processing Technology*, vol. 214, no. 11, pp. 2366–2374, 2014.

[23] P. Singh and D. Dutta, "Multi-direction slicing for layered manufacturing," *Journal of Computing and Information Science in Engineering*, vol. 1, no. 2, p. 129, 2001.

[24] A. Djuric and J. Urbanic, "Design of a Reconfigurable Robot-Based System for Material Deposition Applications," in *2009 IEEE International Conference on Electro/Information Technology*, pp. 458–465, 2009.

[25] S. Keating and N. Oxman, "Compound fabrication : A multi-functional robotic platform for digital design and fabrication," *Robotics and Computer Integrated Manufacturing*, vol. 29, no. 6, pp. 439–448, 2013.

[26] "IRB 1200." ABB, http://new.abb.com/products/robotics/industrial-robots/irb-1200, July 2016.

[27] "ROS: Core Components." http://www.ros.org/core-components/, July 2016.

[28] "Slic3r." http://www.slic3r.org.

[29] "ASTM D638-14, Standard test method for tensile properties of plastics." http://dx.doi.org/10.1520/D0638-14, 2013.

[30] J. F. Rodriguez, J. P. Thomas, and J. E. Renaud, "Mechanical behavior of acrylonitrile butadiene styrene fused desposition materials modeling," *Rapid Prototyping Journal*, vol. 9, pp. 219–230, 2003.